Electronic Supplementary Material

Millisecond synthesis of CoS nanoparticles for highly efficient overall water splitting

Yanan Chen[1,§], Shaomao Xu[1,§], Shuze Zhu[2,§], Rohit Jiji Jacob[3], Glenn Pastel[1], Yanbin Wang[1], Yiju Li[1], Jiaqi Dai[1], Fengjuan Chen[1], Hua Xie[1], Boyang Liu[1], Yonggang Yao[1], Lourdes G. Salamanca-Riba[1], Michael R. Zachariah[3], Teng Li[2], and Liangbing Hu[1] (✉)

[1] *Department of Materials Science and Engineering, University of Maryland College Park, College Park, Maryland 20742, USA*
[2] *Department of Mechanical Engineering, University of Maryland College Park, College Park, Maryland 20742, USA*
[3] *Department of Chemical and Biomolecular Engineering and Chemistry and Biochemistry, University of Maryland College Park, College Park, Maryland 20742, USA*
[§] *Yanan Chen, Shaomao Xu, and Shuze Zhu contributed equally to this work.*

Supporting information to https://doi.org/10.1007/s12274-019-2304-0

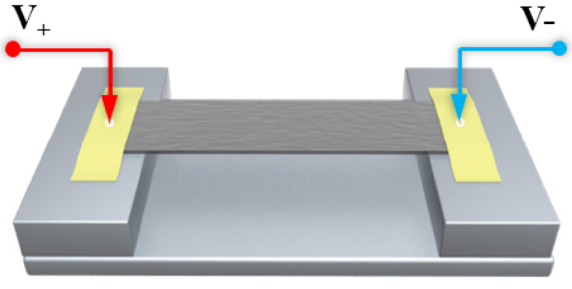

Figure S1 Home-made experimental setup for carrying out the thermal shock high temperature treatment by applying a current or voltage through the samples.

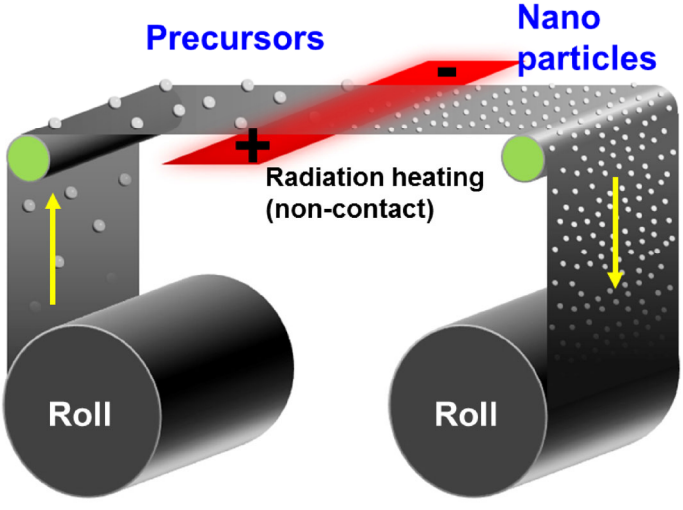

Figure S2 A schematic to show the nanoparticle roll-to-roll manufacturing process induced by thermal shock. As the film passes through the radiation heating zone at a suitable speed, the salts hosted in the RGO matrix are transformed into nanoparticles.

Address correspondence to binghu@umd.edu

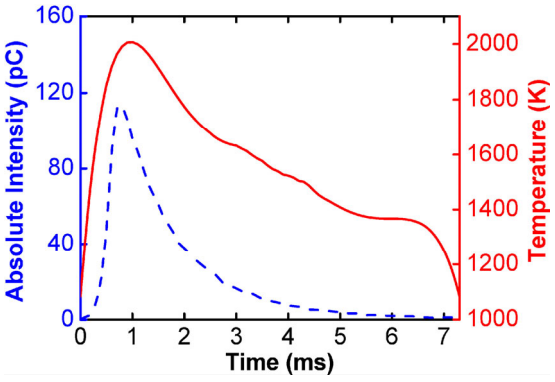

Figure S3 Intensity profile on the 853 nm channel accompanied with temperature in the ultra-fast synthesis process.

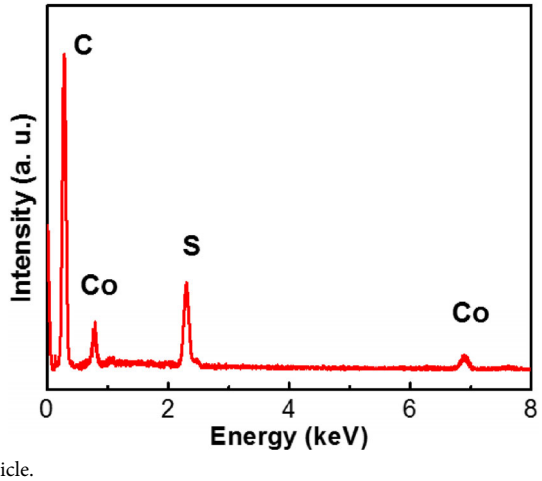

Figure S4 EDX spectra of cobalt-sulfide nanoparticle.

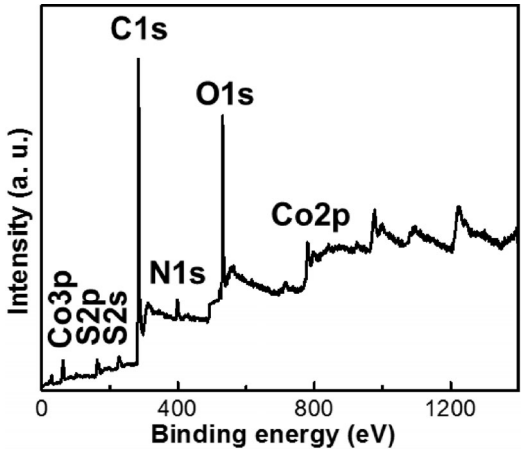

Figure S5 XPS survey spectra of CoS-RGO.

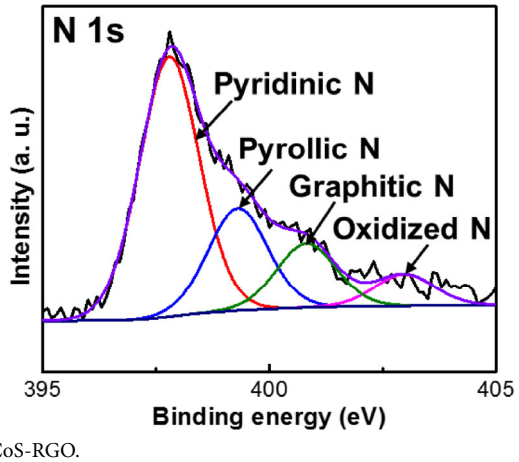

Figure S6 High-resolution N 1s XPS spectrum of CoS-RGO.

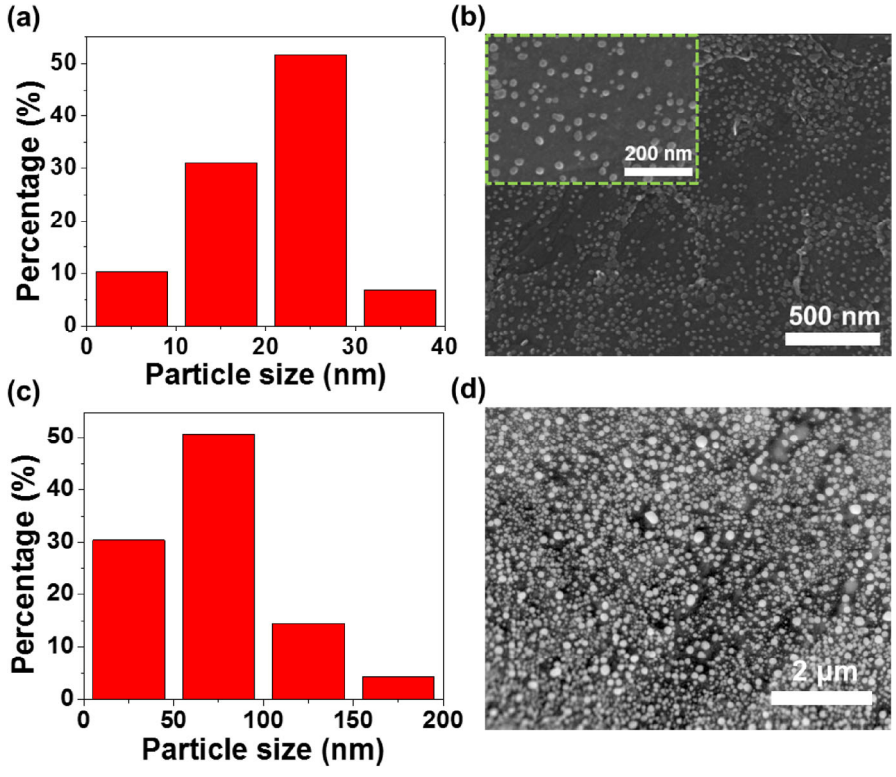

Figure S7 (a) and (b) Statistical particle size distribution and SEM image of CoS nanoparticles loaded on RGO after 7 ms thermal shock treatment. (c) and (d) Statistical particle size distribution and SEM image of CoS nanoparticles loaded on RGO after 5 min thermal shock treatment, which confirms the importance of the short duration in the synthesis of nanoparticles with a small size.

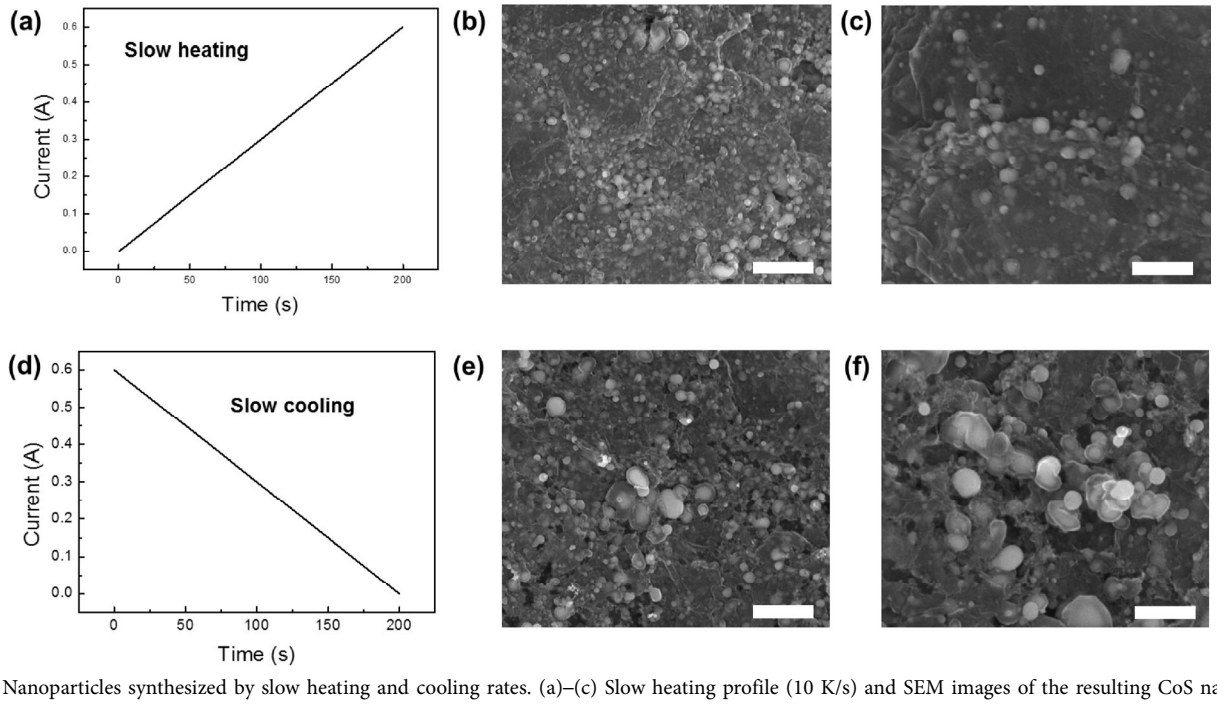

Figure S8 Nanoparticles synthesized by slow heating and cooling rates. (a)–(c) Slow heating profile (10 K/s) and SEM images of the resulting CoS nanoparticles. (d)–(f) Slow cooling profile (10 K/s) and SEM images of the resulting CoS nanoparticles. Scale bars, 1 μm (b, e), 500 nm (c, f).

Figures S10(a) and S10(b) shows the polarization curve and Tafel plot of the CoS-RGO electrocatalyst with a mass loading of 0.5 mg cm^{-2} in 0.5 M H_2SO_4 solution. The CoS-RGO exhibits excellent HER activity with the lowest onset overpotential of 0 mV versus reversible hydrogen electrode (RHE), approaching the performance of commercial 40 wt.% Pt/C and much higher than RGO decorated with Co nanoparticles or nitrogen and sulfur doped RGO, as shown in Figure S10a. Small overpotentials of 17 mV, 74 mV and 149 mV are required for the CoS-RGO electrocatalyst to reach -1, -10 and -100 mA cm^{-2} cathodic currents, respectively, which are among the most active for non-noble material based electrocatalysts (Table S1). In contrast, N- and S-doped RGO need an applied potential of ~540 mV to achieve 10 mA cm^{-2} of cathodic current, and pure RGO film shows negligible activity in the measured voltage range, confirming that such high electrocatalytic performance mainly comes from the synthesized CoS nanoparticles. The corresponding Tafel plot, as depicted in Figure S10(b), shows a small Tafel slope of ~ 56 mV dec^{-1} for CoS-RGO, which is higher than 30.7 mV dec^{-1} for 40 wt% Pt/C electrocatalyst, suggesting a

Volmer-Heyrovsky reaction mechanism. The exchange current density of the CoS-RGO electrocatalyst is obtained as 0.5035 mA cm^{-2} by extrapolating the Tafel plot (Figure S11), which is larger than that of Pt/C with a value of 0.39 mA cm^{-2}. Furthermore, the catalyst exhibits a high turnover frequency (TOF) of 0.1 s^{-1} per active site at 149 mV overpotential (100 mA cm^{-2}), indicating the excellent intrinsic catalytic activity of the as-synthesized CoS-RGO electrocatalyst (Figure S12). Stability is always a critical aspect in catalyst evaluation for long-term application. To assess the durability of the CoS-RGO electrocatalyst in acidic conditions, accelerated linear potential sweeps were carried out continuously at a scan rate of 50 mV s^{-1} (Figure S10c). The polarization curve shows a negligible decay after 500 repeated potential sweeps, which implies that the catalyst is highly stable without any obvious corrosion. Furthermore, the stability of the electrocatalyst is evaluated by electrolysis at fixed potentials over prolonged periods. A stable current density of ~ 20 mA cm^{-2} was observed after 10 h testing at an overpotential of 120 mV (Figure S10(d)). The catalytic current exhibits little loss in the first 2 hours and then fully stabilizes for the rest of the electrolysis.

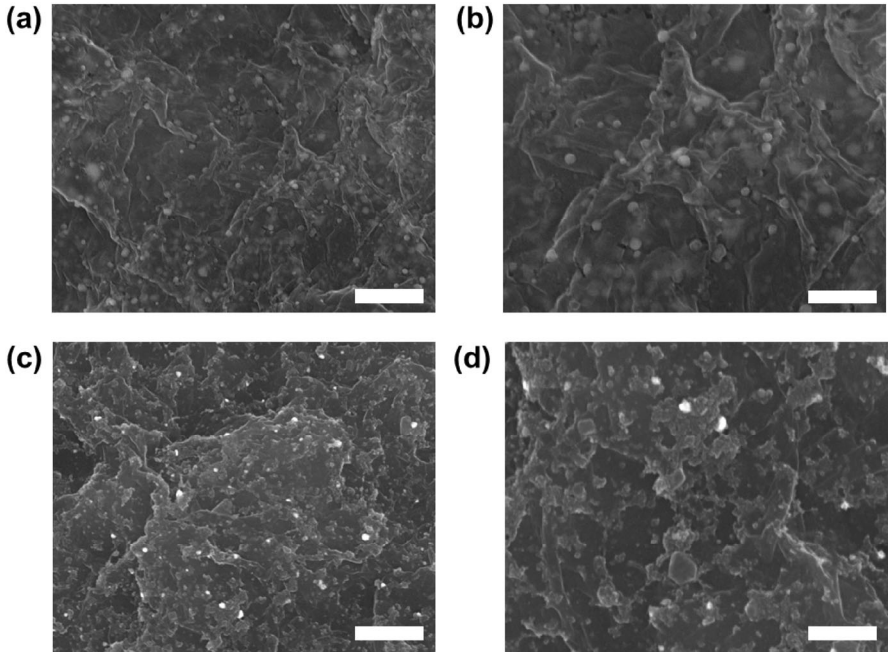

Figure S9 SEM images of the synthesized CoS nanoparticles by 7 ms thermal shock at 1500 K (a) and (b) and 1000 K (c) and (d). Scale bars, 1 μm (a, c), 500 nm (b, d). Compared with thermal shock at 2000 K, a lower thermal shock temperature leads to larger sized particles, which is probably due to the lack of sufficient energy to highly disperse the materials.

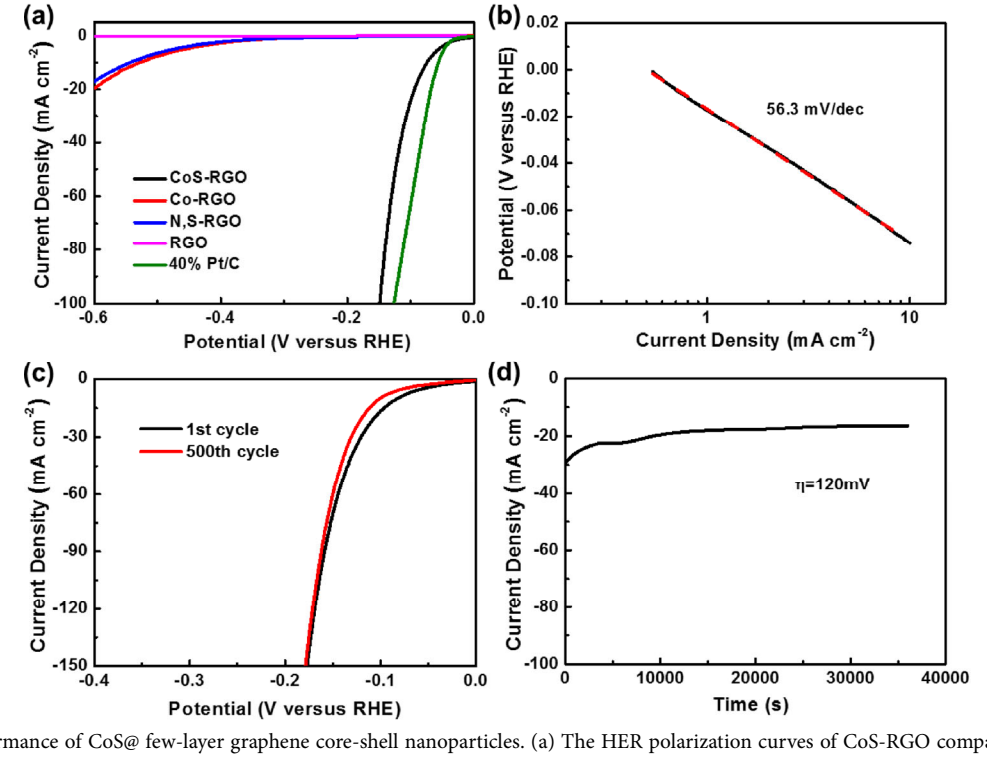

Figure S10 HER performance of CoS@ few-layer graphene core-shell nanoparticles. (a) The HER polarization curves of CoS-RGO compared with RGO, Co-RGO, N,S-RGO at 2 mV s^{-1} in 0.5 M H_2SO_4. (b) Tafel plot of CoS-RGO. (c) Polarization curves after continuous potential sweeps at 50 mV s^{-1} in 0.5 M H_2SO_4. (d) Time dependence of cathodic current density during electrolysis under η = 120 mV in 0.5 M H_2SO_4.

Table S1 Comparison of HER performance in acidic electrolytes for CoS-RGO with state-of-the-art cobalt chalcogenides.

Catalyst	Mass Loading mg cm^{-2}	Onset η (mV)	Tafel Slope (mV decade^{-1})	Current density (j, mA cm^{-2})	η at corresponding j (mV)	Ref
CoS-RGO	0.5	0	56	10 100	74 149	This work
CoS_2/RGO-CNT	1.15	~100	51	10 100	142 178	1
CoS_2	--	60	52	10	190	2
CoS_2 nanowires	1.7	75	52	10	145	3
$CoSe_2$ NP/CP	2.5	~90	42	10 100	137 181	4
CoS_2	0.037	~100	44.6	4	220	5
$Fe_{0.43}Co_{0.57}S_2$	0.037	~100	55.9	4	190	5
CoPS film		~50	57	10	128	6

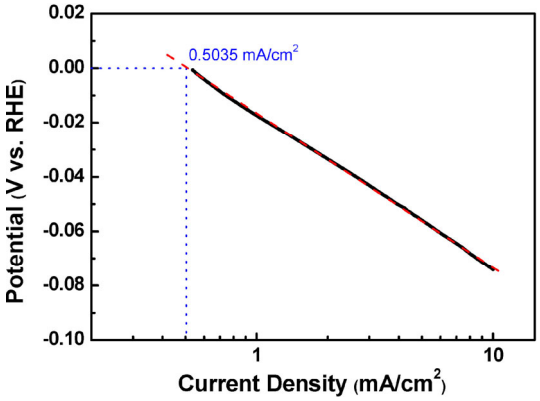

Figure S11 HER Tafel plot of CoS-RGO showing the extrapolation to zero overpotential. The exchange current density was determined to be 0.5035 mA/cm^2.

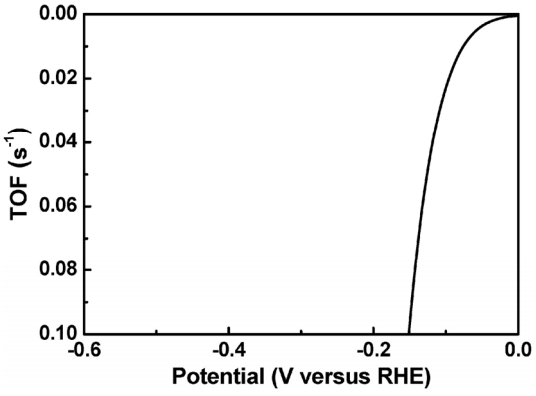

Figure S12 Turnover frequency (TOF) vs. potential in 0.5 M H_2SO_4. TOF = jM/2Fm, where j is the current density, F is Faraday's constant (96485.3 C mol^{-1}), M is the molar mass of CoS, m is the loading mass of CoS, and the number 2 refers to 2 electrons per mole of H_2. According to the inductively coupled plasma emission spectroscopy (ICP) result, the loading mass of CoS is 0.27 mg cm^{-2} derived from the mass ratio of Co (35%).

Table S2 Comparison of OER performance in alkali electrolytes for CoS-RGO with state-of-the-art cobalt chalcogenides and non-noble metal based compounds.

Catalyst	Mass Loading mg cm^{-2}	Tafel Slope (mV decade^{-1})	Current density (j, mA cm^{-2})	η at corresponding j (V)	Ref
CoS-RGO	0.5	71	10 100	1.58 1.66	This work
$Co_{1-x}S$	0.0926	55.6	10	1.6	7
CoP/NCNHP	2	--	10	1.54	8
Co-P/NC	1	52	10	1.55	9
FeNiO	4.12	77	10	1.52	10
CoMoS	2.23	81.3	10	~1.58	11
P-CoMoS	2.19	70.2	10	~1.5	11
N-WC	16	--	10	<1.55	12

Table S3 Comparison of overall water splitting performance in alkali electrolytes for CoS-RGO with state-of-the-art cobalt chalcogenides and non-noble metal based compounds.

Catalyst	Mass Loading mg cm^{-2}	Current density (j, mA cm^{-2})	η at corresponding j (V)	Substrate	Ref
CoS-RGO	0.5	10	1.75	Free-standing	This work
		100	1.97		
N-WC	16	10	<1.5	Free-standing	12
CoP/NCNHP	2	10	1.64	Carbon paper	8
		100	~1.9		
CoSe	3.8	10	1.65	Ti	13
		100	~1.9		
NiFeOx/CNF	1.6	10	1.65	Free-standing	14
	3	10	1.51		
CoOx@CN	2	10	~1.6	Nickel foam	15
$Fe_{0.43}Co_{0.57}S_2$	2.8	10	1.63	Nickel foam	16
MoS_2/Ni_3S_2	9.7	10	1.56	Nickel foam	17
FeNiO	4.12	10	1.46	Nickel foam	10
P-CoMoS	2.19	10	1.54	Free-standing	11

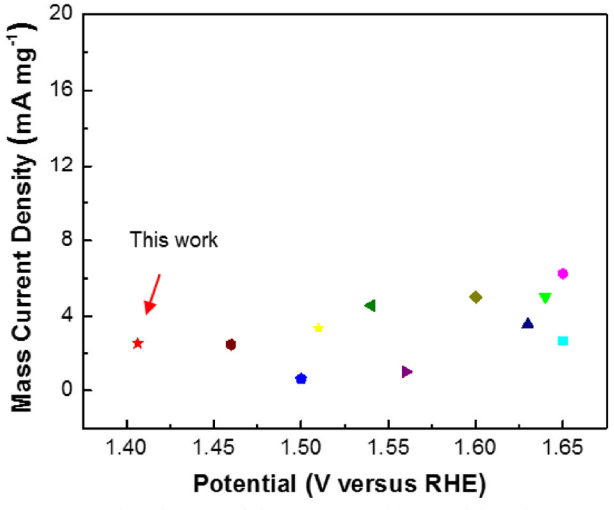

Figure S13 Mass current activity of CoS-RGO compared with state-of-the-art non-noble metal based compounds, indicating the high mass activity of the as-synthesized CoS-RGO catalyst.

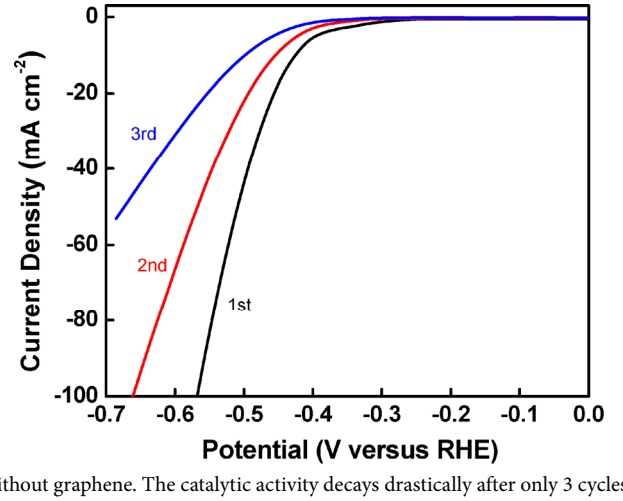

Figure S14 HER polarization curve of CoS without graphene. The catalytic activity decays drastically after only 3 cycles.

Figure S15 (a) shows the top view and side view of a CoS Crystal cell. OA, OB, OC are the cell axes. The length of OA is 0.3367 nm. The length of OB is 0.3367 nm. The length of OC is 0.516 nm. Lattice vector and atom coordinates are displayed as below.

Lattice Vector (Å)			
A=	3.3670000000	0.0000000000	0.0000000000
B=	-1.6835000000	2.9159100000	0.0000000000
C=	0.0000000000	0.0000000000	5.1600000000
Coordinates (Å)			
S	0.0000000000	1.9439383560	1.2900000000
S	1.6835000000	0.9719691780	3.8700000000
Co	0.0000000000	0.0000000000	0.0000000000
Co	0.0000000000	0.0000000000	2.5800000000

The red line in (a) shows the cutting plane to create the surface as used in Figure S15(b) to S15d and main text Figure 6. Figure S15(b) shows the slab model presented in an unit cell from different viewing perspectives (these viewing perspectives also apply to the remaining of this supplementary information). The unit cell has the following geometrical size: a (along OA direction) = 2.3569 nm, b (along OB direction) = 0.3367 nm, c (along OC direction) = 0.516nm; alpha = 90 degrees, beta = 90 degrees, gamma = 120 degrees. There are 9 water molecules filling up the vacuum space. The geometrical dimension of the vacuum space along OA direction is 1.6835 nm, giving a water density 1.0631 g/cm^3. 1x7x5 Monkhorst-Pack k-points are used. Please note that all calculations are performed using the unit cell model but the presentation may be in a supercell for visual clarity as explained next. Figure S15(c) shows the slab model presented in a supercell. The grey box schematics shows the zoomed region for display in main text Figure 6. Similar definition of the zoomed view also applies to the remaining of this supplementary information.

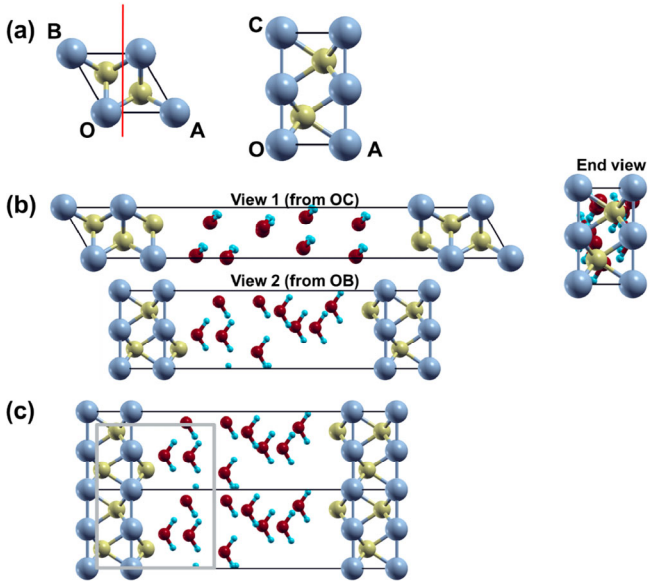

Figure S15 (a) An unit cell for the CoS crystal. The red line shows the cutting plane to create the slab model. (b) A slab model with three perspective views. This model is used for main text Figure 6. (c) The slab model presented in a supercell. The grey box schematics shows the zoomed region for display in main text Figure 6.

Figure S16 shows the multiple rounds of Volmer reactions on the surface as shown in Figure 6 in main text from two viewing perspectives in a zoomed view. Figure S16(a) shows that two pairs of protons and electrons (two additional hydrogen atoms) are added to the unit cell for the starting round of simulation. Two H are adsorbed on Co and S respectively. Figure S16(b) shows that, after adding a new pair of proton and electron (one additional hydrogen atom), we don't see the adsorption of the H on to the catalyst surface. Instead, we observe that the H that initially adsorbed on S has changed its adsorption site to Co. This also suggests that the H adsorbed on S is much more active than those adsorbed on Co. Figure S16(c) shows that, after adding a new pair of proton and electron (one additional hydrogen atom), a H is adsorbed on S. This is the last round of simulation before the production of hydrogen molecules occurs (see Figure 6 in main text) if further adding new pair of proton and electron.

Figure S17 shows geometry-optimized structures of the slab model, without water molecules filling the vacuum. These are the structures used for DOS calculations as in Figure 6. Moderate changes on the surface morphology upon hydrogen adsorption are seen. 10x70x50 k-points are used for calculating the DOS.

Note that we do not observe the apparent Tafel reaction, which requires two adsorbed hydrogen atoms. Since an S site usually can only accommodate one hydrogen atom, at least one of these two hydrogen atom has to be from these adsorbed on Co. The fact that the Co site is less active could possible hinder the Tafel reaction.

Figure S18(a) shows two other cutting planes to have only S or Co exposed for reaction. The slab models are created in a similarly way as shown in Figure S16. The unit cell of slab model has the following geometrical size: a (along OA direction) =0.3367 nm, b (along OB direction) =0.3367 nm, c (along OC direction) =2.58 nm; alpha=90 degrees, beta=90 degrees, gamma=120 degrees. There are 5 water molecules filling up the vacuum space. The geometrical dimension of the vacuum space along OA direction is 1.548 nm, giving a water

density 0.9843 g/cm^3. 7x7x1 Monkhorst-Pack k-points are used. Figure S18b shows that after two rounds of AIMD simulations, the Co is hydrogenated with two H atoms. Figure S18(c) shows that further adding of H atom does not trigger the production of hydrogen molecule. The Co is still hydrogenated with two H atoms. Figure S18(d) shows that in a similar setup but using the S exposed surfaces, the HER could easily occur. The above also demonstrates that S is the active site. Figure S19 presents the DOS calculations on these two types of surfaces.

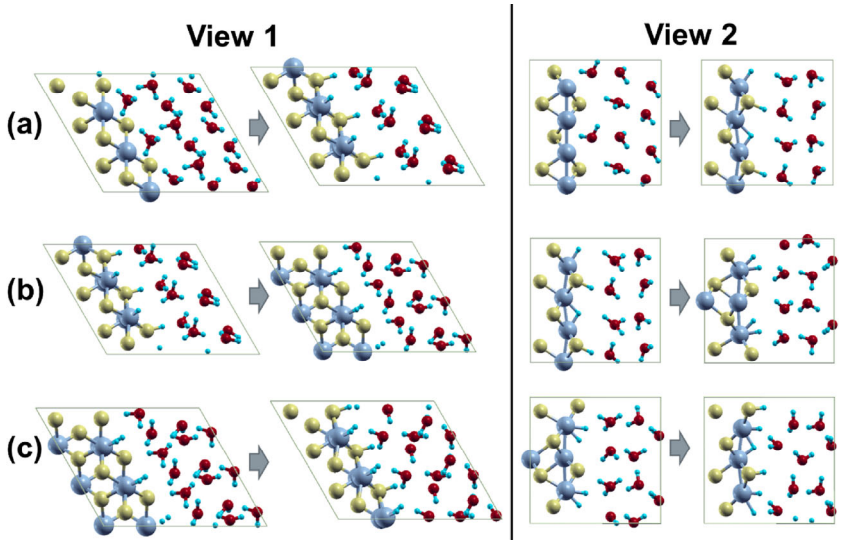

Figure S16 Multiple rounds of Volmer reactions on the surface as shown in Figure 6 in the main text from two viewing perspectives in a zoomed view.

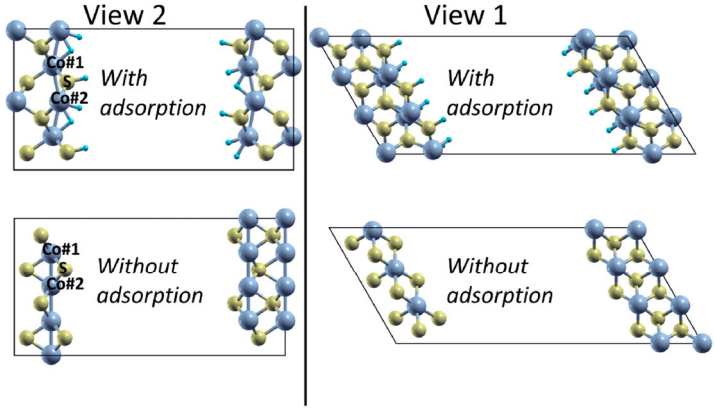

Figure S17 Geometry-optimized structures of the slab model without water, which are used for DOS calculation.

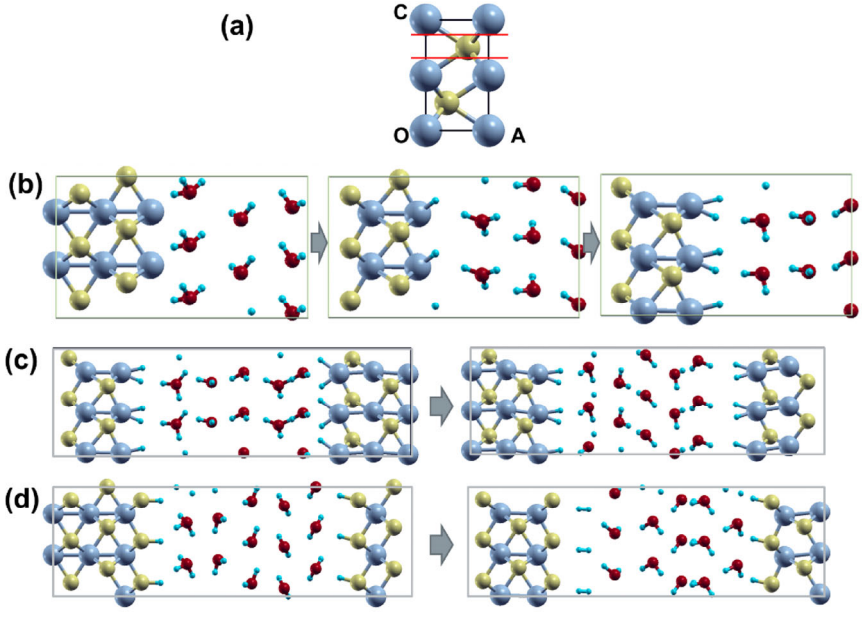

Figure S18 (a) Schematic showing the generation of new types of surfaces from CoS crystal. Red lines denote the cutting plane. (b) The Co is hydrogenated with two H atoms after two rounds of simulating Volmer reaction. (c) Further adding of H atom doesn't trigger the production of hydrogen molecule on Co exposed surface. (d) HER could easily occur on S exposed surfaces.

Figure S19(a) shows the DOS calculated for the Co exposed surface with and without hydrogen adsorption. The calculation is performed in a similar way as in Figure S17. 70x70x10 k-points are used for calculating the DOS. It shows that there is no apparent peak of anti-bonding states of Co emerging above the Fermi level upon hydrogen adsorption. On the contrary, Figure S19(b) shows that there is an apparent peak of anti-bonding states of Co emerging above the Fermi level upon hydrogen adsorption. This supports that S is a more active reaction site than Co.

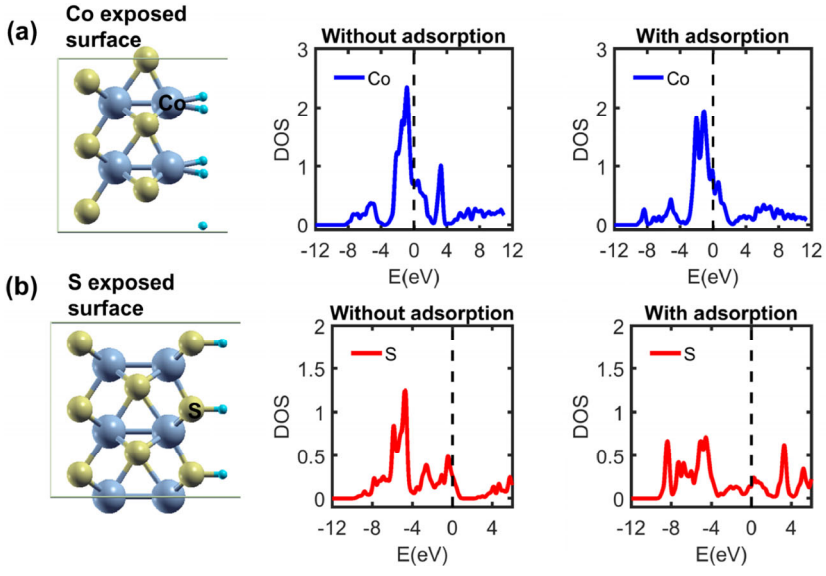

Figure S19 (a) DOS calculated for the Co exposed surface with and without hydrogen adsorption. (b) DOS calculated for the S exposed surface with and without hydrogen adsorption.

References

[S1] Peng, S.; Li, L.; Han, X.; Sun, W.; Srinivasan, M.; Mhaisalkar, S. G.; Cheng, F.; Yan, Q.; Chen, J.; Ramakrishna, S. Cobalt Sulfide Nanosheet/graphene/carbon Nanotube Nanocomposites as Flexible Electrodes for Hydrogen Evolution. *Angew. Chem. Int. Ed Engl.* **2014**, *53*, 12594–12599.

[S2] Faber, M. S.; Lukowski, M. A.; Ding, Q.; Kaiser, N. S.; Jin, S. Earth-Abundant Metal Pyrites (FeS2, CoS2, NiS2, and Their Alloys) for Highly Efficient Hydrogen Evolution and Polysulfide Reduction Electrocatalysis. *J. Phys. Chem. C* **2014**, *118*, 21347–21356.

[S3] Faber, M. S.; Dziedzic, R.; Lukowski, M. A.; Kaiser, N. S.; Ding, Q.; Jin, S. High-Performance Electrocatalysis Using Metallic Cobalt Pyrite (CoS2) Micro- and Nanostructures. *J. Am. Chem. Soc.* **2014**, *136*, 10053–10061.

[S4] Kong, D.; Wang, H.; Lu, Z.; Cui, Y. CoSe2 Nanoparticles Grown on Carbon Fiber Paper: An Efficient and Stable Electrocatalyst for Hydrogen Evolution Reaction. *J. Am. Chem. Soc.* **2014**, *136*, 4897–4900.

[S5] Kong, D.; Cha, J. J.; Wang, H.; Lee, H. R.; Cui, Y. First-Row Transition Metal Dichalcogenide Catalysts for Hydrogen Evolution Reaction. *Energy Environ. Sci.* **2013**, *6*, 3553–3558.

[S6] Cabán-Acevedo, M.; Stone, M. L.; Schmidt, J. R.; Thomas, J. G.; Ding, Q.; Chang, H.-C.; Tsai, M.-L.; He, J.-H.; Jin, S. Efficient Hydrogen Evolution Catalysis Using Ternary Pyrite-Type Cobalt Phosphosulphide. *Nat. Mater.* **2015**, *14*, 1245–1251.

[S7] Xu, Y.; Hao, Y.; Zhang, G.; Jin, X.; Wang, L.; Lu, Z.; Sun, X. One-Step Scalable Production of Co1− X S/Graphene Nanocomposite as High-Performance Bifunctional Electrocatalyst. *Part. Part. Syst. Charact.* **2016**, *33*, 569–575.

[S8] Pan, Y.; Sun, K.; Liu, S.; Cao, X.; Wu, K.; Cheong, W.-C.; Chen, Z.; Wang, Y.; Li, Y.; Liu, Y.; et al. Core–Shell ZIF-8@ZIF-67-Derived CoP Nanoparticle-Embedded N-Doped Carbon Nanotube Hollow Polyhedron for Efficient Overall Water Splitting. *J. Am. Chem. Soc.* **2018**, *140*, 2610–2618.

[S9] You, B.; Jiang, N.; Sheng, M.; Gul, S.; Yano, J.; Sun, Y. High-Performance Overall Water Splitting Electrocatalysts Derived from Cobalt-Based Metal–Organic Frameworks. *Chem. Mater.* **2015**, *27*, 7636–7642.

[S10] Qian, M.; Cui, S.; Jiang, D.; Zhang, L.; Du, P. Highly Efficient and Stable Water-Oxidation Electrocatalysis with a Very Low Overpotential Using FeNiP Substitutional-Solid-Solution Nanoplate Arrays. *Adv. Mater.* **2017**, *29*, 1704075.

[S11] Ray, C.; Lee, S. C.; Sankar, K. V.; Jin, B.; Lee, J.; Park, J. H.; Jun, S. C. Amorphous Phosphorus-Incorporated Cobalt Molybdenum Sulfide on Carbon Cloth: An Efficient and Stable Electrocatalyst for Enhanced Overall Water Splitting over Entire pH Values. *ACS Appl. Mater. Interfaces* **2017**, *9*, 37739–37749.

[S12] Han, N.; Yang, K. R.; Lu, Z.; Li, Y.; Xu, W.; Gao, T.; Cai, Z.; Zhang, Y.; Batista, V. S.; Liu, W.; et al. Nitrogen-Doped Tungsten Carbide Nanoarray as an Efficient Bifunctional Electrocatalyst for Water Splitting in Acid. *Nat. Commun.* **2018**, *9*, 924.

[S13] Liu, T.; Liu, Q.; Asiri, A. M.; Luo, Y.; Sun, X. An Amorphous CoSe Film Behaves as an Active and Stable Full Water-Splitting Electrocatalyst under Strongly Alkaline Conditions. *Chem. Commun.* **2015**, *51*, 16683–16686.

[S14] Wang, H.; Lee, H.-W.; Deng, Y.; Lu, Z.; Hsu, P.-C.; Liu, Y.; Lin, D.; Cui, Y. Bifunctional Non-Noble Metal Oxide Nanoparticle Electrocatalysts through Lithium-Induced Conversion for Overall Water Splitting. *Nat. Commun.* **2015**, *6*, 7261.

[S15] Jin, H.; Wang, J.; Su, D.; Wei, Z.; Pang, Z.; Wang, Y. In Situ Cobalt–Cobalt Oxide/N-Doped Carbon Hybrids As Superior Bifunctional Electrocatalysts for Hydrogen and Oxygen Evolution. *J. Am. Chem. Soc.* **2015**, *137*, 2688–2694.

[S16] Tang, C.; Cheng, N.; Pu, Z.; Xing, W.; Sun, X. NiSe Nanowire Film Supported on Nickel Foam: An Efficient and Stable 3D Bifunctional Electrode for Full Water Splitting. *Angew. Chem. Int. Ed.* **2015**, *54*, 9351–9355.

[S17] Zhang, J.; Wang, T.; Pohl, D.; Rellinghaus, B.; Dong, R.; Liu, S.; Zhuang, X.; Feng, X. Interface Engineering of MoS2/Ni3S2 Heterostructures for Highly Enhanced Electrochemical Overall-Water-Splitting Activity. *Angew. Chem. Int. Ed.* **2016**, *55*, 6702–6707.